26th Symposium on Naval Hydrodynamics
Rome, Italy, 17-22 September 2006

Resistance Predictions of High Speed Mono and Multihull Ships with and without Water Jet Propulsors using URANS

R. Miller, J. Gorski
(Naval Surface Warfare Center, Carderock Division, USA)
T. Xing, P. Carrica, F. Stern
(The University of Iowa, Iowa City, USA)

ABSTRACT

Resistance, sinkage, and trim calculations are performed over large ranges of speeds for the Athena R/V Model 5365 and the high speed sealift trimaran concept Model 5594 using the Unsteady Reynold's Averaged Navier Stokes (URANS) solver CFDShip-Iowa. Steady state resistance values for individual speeds are calculated with the hulls free to sink and trim or fixed at a given sinkage and trim. Full speed range resistance curves are obtained using a "numerical tow tank" concept by slowly accelerating the ship from Fr = 0.0 to 1.0. The calculated resistance, sinkage, and trim values are compared with experimental measurements. Free surface wave cuts and wave profiles are also compared.

Self-propulsion of the Athena R/V appended with skeg, stabilizers, shafts, struts, and rudders is simulated for two Froude numbers in the free to sink and trim mode. The predicted terminal Froude number, sinkage, and trim values are compared with the experiment.

Preliminary calculations for the Athena R/V fitted with waterjets are performed, demonstrating CFDShip-Iowa's ability to simulate this configuration. Streamlines and free surface plots illustrate the above waterline jet discharge impacting the transom wake. Differences with the calculated nojet transom wake are shown.

INTRODUCTION

There is a growing interest in high-speed sealift ships ranging in speeds from 40 up to 70 knots. These speeds are significantly greater than many of the conventional sealift ships of today. Slender monohulls and multihulls are under consideration to meet these requirements. Waterjets are often proposed as the means of propulsion for such craft. Waterjet systems are much different than conventional open propellers and the propulsor/hull interactions of such systems are clearly different. There is limited experience and experimental data for such craft and it is important to have computational tools that can be used to accurately evaluate these new concepts.

First and foremost is the accurate prediction of the resistance for these hulls. Reynold's Averaged Navier Stokes (RANS) solvers have been used in the past to predict resistance for ship hulls. Predictions, by Miller et al. (2005) and others, of the Model 5415 were submitted as part of the ONR Tokyo 2005 workshop (Hino, 2005). This hull was, however, held fixed at a *given sinkage and trim* for a single Fr = 0.28. It is desirable to predict the resistance and powering for ships over the entire speed range where the wave pattern and ship orientation change dramatically. Because the resistance depends significantly on the sinkage and trim, particularly for high speed craft, it is important for the ship to have the correct orientation. Additionally, realistic simulations depend on accurate representations of the actual hull being tested. Multihull interaction and propulsors add more complexity to the configurations computed.

Advancements in the capabilities of CFDShip-Iowa in recent years have addressed these issues, expanding the domain of Naval Ship Hydrodynamics problems for which it can be used effectively (Carrica et al., 2006a). Previous versions of the code (Paterson et al., 2003) used the free surface tracking boundary condition, where a parameter surface of the computational grid conforms

to the free surface. Grid parameter lines in the other direction lengthen or shorten and the grid spacing expands or contracts where necessary to create a modified computational volume, while keeping the original grid topology intact. When the free surface waves produced or encountered and/or body motions are substantial, the wetted hull surface changes dramatically, requiring substantial regridding of the body fitted surface grids. If the change in wetted area is too great, the solver will not be able to regrid the surface or the resulting poor grid quality will cause the computation to fail. The introduction of the level-set free surface technique has eliminated this problem, since regridding of the computational volumes is not required. Additionally, level-set free surfaces can be used to predict highly distorted interfacial topologies such as breaking waves and wet/dry transom stern flows and the above-water discharge produced by some waterjet propulsors.

The addition of overset grid technology addresses many of the difficulties inherent in the simulations. The first is the ability to add refinement blocks in areas where more grid resolution is required to predict detailed physics. Figure 1 illustrates the level-set overturning bow wave prediction shown at the ONR Athena Wave Breaking Workshop. For this calculation two levels of embedded refinement were added to predict the overturning bow wave. (The hull was held at fixed sinkage and trim in this calculation). The results from these calculations and others are discussed by Wilson et al. (2006). Secondly, the grid creation for complex hull configurations such as ships appended with shafts and struts or waterjets can be dealt with effectively. Thirdly, the addition of dynamic overset grids allows for the independent motion of bodies (structured grid blocks) which are embedded in a fixed background grid. The motion of these bodies can be prescribed or predicted by a 6 DOF solver. The dynamic sinkage and trim is predicted in this way.

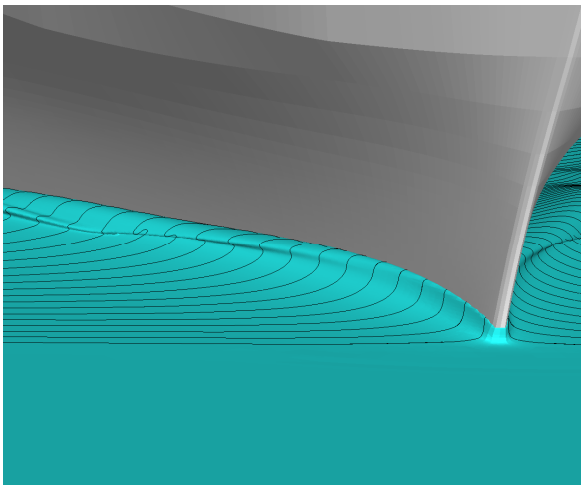

Figure 1: Athena Breaking Bow Wave

Details of CFDShip-Iowa version 4 will be discussed next, along with examples of full speed range predictions of the resistance, sinkage and trim for the trimaran Model 5594 and the monohull Athena. Propulsor examples will include powering predictions for the Athena hull appended with shafts, struts and rudders and preliminary investigations of the Athena model installed with waterjets including above waterline discharge.

URANS SOLVER – CFDShip-Iowa Details

Calculations performed in this paper use the URANS solver CFDShip-Iowa, version 4. Details of the solution algorithm and mathematics can be found in numerous references, including Carrica et al. (2006a, 2006b, 2006c). CFDShip-Iowa is a general-purpose research URANS computational fluid dynamics code developed at the University of Iowa for support of student thesis and project research at the university as well as transition to Naval laboratories. Basic solver numerical modeling details include 2^{nd} order upwind convective terms and 2^{nd} order central differenced viscous terms. The velocity and pressure are coupled using a PISO algorithm. For the time derivatives a 2^{nd} order backward difference is used. Advanced iterative solvers available in the PETSC toolkit are used to solve the Poisson (elliptic) pressure equation. Turbulence modeling uses Menter's blended k-w/k-e model (Menter, 1994). The solver uses MPI-based domain decomposition for parallel processing. Ghost cells are used to retain high order stencils across split block boundaries. The addition of multiple-body specification allows bodies to move independently of

one another and individual body surface force integrations for force analysis can be obtained.

Overset grids are being used in a wide variety of ways ranging from calculations of a static bare hull embedded in a background grid to dynamically moving fully appended ships. Dynamic overset grids allow for the relative motion between blocks. Additionally, overset grids remove the necessity of point-to-point matching in structured grid systems. This alleviates some of the difficulties involved in creating structured grids about complex configurations such as hulls appended with shafts and struts or waterjets. Multihull and multiple body grid configurations are much more easily created. Refinement blocks can be added to resolve flow features not resolved by the base grid. The grid assemble tool used is SUGGAR by Noack (2005). SUGGAR is used to blank (turn off) points inside closed solid boundaries and to establish communication between overlapping grids via fringe points and donor cells. SUGGAR is run as a preprocessor for static calculations or concurrently with CFDShip-Iowa for simulations using dynamic grid motions. Communication and synchronization between CFDShip-Iowa and SUGGAR uses a UNIX FIFO (first-in/first-out) communication pipe. In both cases the familiar XINTOUT file is created containing the grid assembly information. The software, USURP, developed by Boger and Dreyer (2006), is used to properly compute area and forces on overlapping surface regions.

Typically, for 6DOF problems, hull and appendage overset blocks are designated to be moving, while a background block remains fixed. The motion of the moving bodies can be prescribed with user input or predicted by the solution of the rigid body equations of motion. The code allows for explicit or implicit predicted motion at each time step. At each time step the surface and body forces and moments are obtained for each object. The rigid body equations of motion are then solved for the motions. The solver updates the translation and rotation of the moving grids and sends the motions to SUGGAR to create the new grid assembling information. Sinkage and trim predictions are obtained in this way. To compute the resistance, sinkage, and trim at a single speed, the Froude and Reynold's numbers are set to their appropriate values and then the solution is started abruptly from some initial values with the hull in its initial static condition. The URANS solver continues while updating the hull's orientation until steady state values of resistance, sinkage and trim occur. At low speeds, the motion will oscillate about some average value due to the unsteady hydrodynamic forces.

Instead of making multiple steady state runs at different Froude numbers, CFDShip-Iowa has the capability to predict sinkage and trim for a full range of Froude numbers (for example 0 to 1) in a single-run using a slow speed ramp. This means the ship will be accelerated slowly from a low Froude number to a high Froude number during a slow time ramp. It is expected that any points during the computation will be very close to the "steady state" solution at that Froude number as long as the time ramp is slow enough to make the effect of acceleration negligible. From the mathematical point of view, this means the time derivatives of the momentum, level set transport, and turbulence model equations are nearly zero:

$$\mathbf{v}\cdot\nabla\mathbf{v} = -\nabla p + \nabla\cdot\left[\frac{1}{\mathrm{Re}_{eff}}\left(\nabla\mathbf{v}+\nabla\mathbf{v}^{T}\right)\right] + \mathbf{S} \tag{1}$$

$$\mathbf{v}\cdot\nabla\phi = 0 \tag{2}$$

$$\left(\mathbf{v}-\sigma_k\nabla\nu_t\right)\cdot\nabla k - \frac{1}{P_k}\nabla^2 k + s_k = 0 \tag{3}$$

$$\left(\mathbf{v}-\sigma_\omega\nabla\nu_t\right)\cdot\nabla\omega - \frac{1}{P_\omega}\nabla^2\omega + s_\omega = 0 \tag{4}$$

The level of accuracy in this numerical towing tank computation depends on the acceleration imposed. A trade off between computation speed and negligibility of the time derivatives is necessary. The physical characteristic times involved in the process of reaching steady-state are the times necessary to form the boundary layer and to develop the Kelvin wave. These two times are in the order of the time needed to cover one ship length. So during this time we would like the change of ship speed to be small, to obtain essentially constant speed values of resistance, sinkage and trim. If the acceleration to full speed ($U_0 = 1$ corresponds to $Fr_{\max}$) is linear,

$$U = \frac{t}{T} = \frac{Fr}{Fr_{\max}} \tag{5}$$

where T is the nondimensional time to reach maximum speed. To cover one ship length the ship needs to travel a time Δt obtained from:

$$1 = \int_{t-\Delta t/2}^{t+\Delta t/2} t/T \, dt = \frac{t}{T}\Delta t \tag{6}$$

and using Eqs. (5) and (6) we obtain the change of Froude number to cover one ship length:

$$\Delta Fr = \frac{Fr_{\max}^2}{T\, Fr} \tag{7}$$

which shows that the change in the Froude number while the ship travels a ship length is proportional to the inverse of the period and the instantaneous Froude number.

Self-propulsion is simulated using a simplified body-force model for propeller (Stern, 1988). This model requires the input of thrust, torque and advance coefficients for the propeller. For a typical steady state computation at one specific Froude number, the ship speed is initially set to zero. When the propeller is turned on, the ship accelerates until it reaches a constant speed when the resistance force balances the thrust force from propeller. Usually EFD data are reported in full scale and then need to be converted back to model scale, which is briefly summarized below**:**

1. First assume the thrust deduction *t*, wake factor *1-wt*, and propeller open water curves are the same for ship scale and model scale.
2. From the full scale effective power P_{ES} and ship Velocity V_S, the total resistance force can be computed:

$$R_{TS} = P_{ES}/V_S \tag{8}$$

3. The residual resistance is:

$$C_R = C_{TS} - C_{AS} - C_{FS} \tag{9}$$

where C_{AS} is the correlation allowance (0.0005) and friction coefficient C_{FS} is computed using the ITTC friction line (ITTC, 1957):

$$C_{FS} = \frac{0.075}{\left(\log_{10} \mathrm{Re}_S - 2\right)^2} \tag{10}$$

4. Using the Froude number similarity and the length of the model, the model velocity can be computed and thus the model Reynolds number

$$V_M = Fr\sqrt{gL_M} \Rightarrow \mathrm{Re}_M \tag{11}$$

The friction coefficient is:

$$C_{FM} = \frac{0.075}{\left(\log_{10} \mathrm{Re}_M - 2\right)^2} \tag{12}$$

Other definitions follow. The total resistance coefficient is:

$$C_{TM} = C_{FM} + C_R \tag{13}$$

The total resistance force on the model is:

$$R_M = \frac{1}{2}\rho S_{WET} V_M^2 C_{TM} \tag{14}$$

The wake velocity V_{AM} is defined as :

$$V_{AM} = V_M\left(1 - WT\right) \tag{15}$$

and the total thrust force needed from the propeller is:

$$T_M = \frac{\left(R_M - SFC\right)}{2\left(1-t\right)} \tag{16}$$

Finally, the skin friction correction *SFC* is defined as:

$$SFC = \frac{1}{2}\rho_M V_M^2 S_M \left(C_{FM} - C_{FS} - C_{AS}\right) \tag{17}$$

The propeller open water curves can be fitted with a parabola to simplify computations. Then the advance coefficient J_M can be computed:

$$a_M = C_{TTM} = \frac{T_M}{\rho_M V_M^2 {D_M}^2}$$
$$\left(a_M + 0.0408\right){J_M}^2 + 0.495 J_M - 0.614 = 0 \tag{18}$$

RPM of propeller *n* is computed from velocity V_M, advance coefficient J_M and propeller diameter D_M:

$$n = \frac{V_M}{J_M D_M} \tag{19}$$

and the torque coefficient is:

$$K_{Q0M} = (1.043 - 0.807 J_M - 0.0372 {J_M}^2)/10 \tag{20}$$

$$K_{QM} = \frac{K_{Q0M}}{\eta_R} \tag{21}$$

Similarly, the thrust coefficient of the propeller K_{TM} and C_{TM} are:

$$K_{TM} = \frac{T_M}{\rho n^2 D_M{}^4} = \frac{T_M}{\rho V_M^2 D_M{}^2} \frac{V_M^2}{n^2 D_M{}^2} = C_{TTM} J_M{}^2 \tag{22}$$

$$C_{TM} = \frac{8}{\pi J_M{}^2} K_{TM} \tag{23}$$

Trimaran – Model 5594

Model experiments were performed on Model 5594 representing the conceptual design of a high speed sealift trimaran (Kennel, 2004). Figure 2 shows a sketch and the bodyplan of the trimaran. The waterline length at design conditions is 313 m. and the overall beam is 39.2 m. The centerhull beam is 18.8 m. The slenderness ratio for the centerhull is 16.65. The hull has a large deeply immersed transom. The sidehulls represent less than 2% of the overall displacement. The model is 1:45 scale. The sidehulls are 51m long and positioned at the aft end of the Trimaran, and have a deep draft. Resistance, sinkage and trim were measured for a range of speeds: 25 to 80 kts. full scale, corresponding to Froude numbers .23 to .74. The model Reynolds

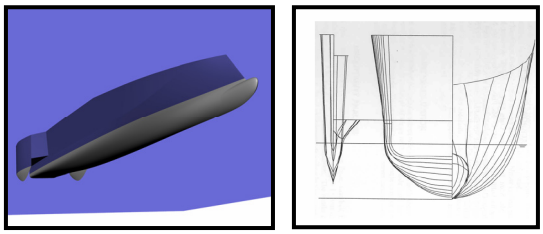

Figure 2: Sketch of the Model 5594 trimaran and body plan.

numbers ranged from 13.3 to 43 Million. Model scale frictional resistance was obtained from ITTC. Wavecut data was obtained for 45 kts., 55 kts. and 65 kts full scale. Numerous configurations of the trimaran were tested including the centerhull alone to look at the impact of the sidehulls on the resistance and flow field of the trimaran. For speeds above 50 kts. a significant amount of side hull generated spray was observed impinging on the above waterline hull. The significant increase in wetted area resulted in increased drag at these speeds. Simple spray rails were added to deflect the spray which resulted in a lower drag. The hulls were tested in 3 different draft conditions in both calm and rough seas: full load even keel and mid-voyage loading conditions at two different trims.

Calculations were performed with CFDShip-Iowa to evaluate its capability at predicting resistance, sinkage and trim over a wide range of speeds in calm seas for the multihull and monohull geometries of the Model 5594. The monohull and trimaran configurations simulated correspond to the static full load, even trim, condition. Hull loading characteristics and mass properties relevant to this configuration are shown in Table 1. Spray rails were not included in the calculation.

Draft (Bow)	Draft (Stern)	VCG	LCG	Pitch gyradius
0.027	0.027	0.0033 above WL	0.0147 aft of midships	0.27

Table 1: Model 5594 – Full Load, Even Trim Condition

For accurate resistance predictions, the hulls must be in the correct trim position. The trim condition varies greatly over the speed range. Resistance calculations were first performed over the speed range for the hulls in a *fixed sinkage and trim* condition given from the measured values. At each speed the calculation was run to steady state. Secondly, the hulls were *free to sink and trim* in response to the calculated hydrodynamic forces over the speed range using the procedure described earlier. Additional full unsteady runs were performed to spot check quasi-steady runs.

Fixed Sinkage & Trim – Predicted Resistance

The grid topology and individual grid extents used for these calculations are shown in Figure 3. Since port-starboard symmetry is imposed, only half of the flow domain is discretized. The basic system is composed of 4 blocks: 1) Centerhull block, 2&3) sidehull blocks, and a background grid. Table 2 shows the block sizes and block partition sizes for the system.

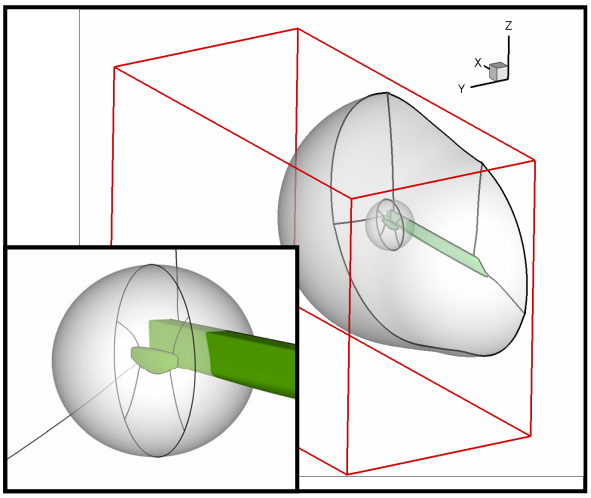

Figure 3: Model 5594 grid extents.

Name	# Grid Pts	# Blocks	# Pts/Block
Centerhull	1,398,813	16	87,425.81
Sidehull - Inboard	333,775	4	83,443.75
Sidehull - Outboard	333,775	4	83,443.75
Background	2,037,776	24	84,907.33
Total Assembly	4,104,139	48	85,502.90

Table 2: Model 5594 grid assembly.

The error in the discretization of the centerhull and sidehulls static wetted area is 0.44% and 0.27% respectively. The background grid extends about 1 ship length forward of the bow, 1.5 ships aft of the stern, and about 1 length to the side. At each speed the bow and stern rises and the resulting trims were measured in the experiment. Given this information, SUGGAR was run as preprocessor to sink and trim the geometry and to produce the grid assembly information used by CFDShip-Iowa. Figure 4 illustrates the assembly in two vertical cuts through the grid. The longitudinal cut near the centerplane shows the assembly between the centerhull block and the background grid and the tranverse cut shows the assembly between the sidehull, centerhull, and background. These illustrate the inner hole fringe (boundary) points in the background grid and the outer fringe (boundary) points of the sidehull and centerhull grids.

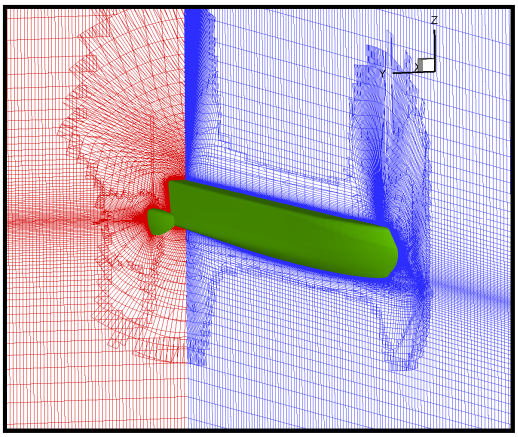

Figure 4: Model 5594: SUGGAR grid assembly.

Figure 5 shows the computed free surface elevations for both the monohull and trimaran at Fr = 0.511. As seen in the figures, the small side hull is embedded in the Froude number dependent wave field produced by the much larger center hull. The interference of the two wave patterns can be seen downstream of the hulls. Additional effects due to the sidehulls can be seen, Figure 6, in the modified pressure distribution on the centerhull. Figures 7 and 8 show wavecut comparisons for the monohull and trimaran at y/L = 0.081, 0.102, 0.294, and y/L = 0.335. The locations of these cuts are shown with dashed lines in Figure 5. The calculation predicts the height and phase of the larger waves very well , but does not resolve the small waviness between x/L = 0.6 and 1.25 for y/L = 0.081 and 0.102. Refinement blocks are probably necessary to compute these small waves. This was seen in previous calculations of the Model 5415, see Wilson et al. (2006) and Miller et al. (2005).

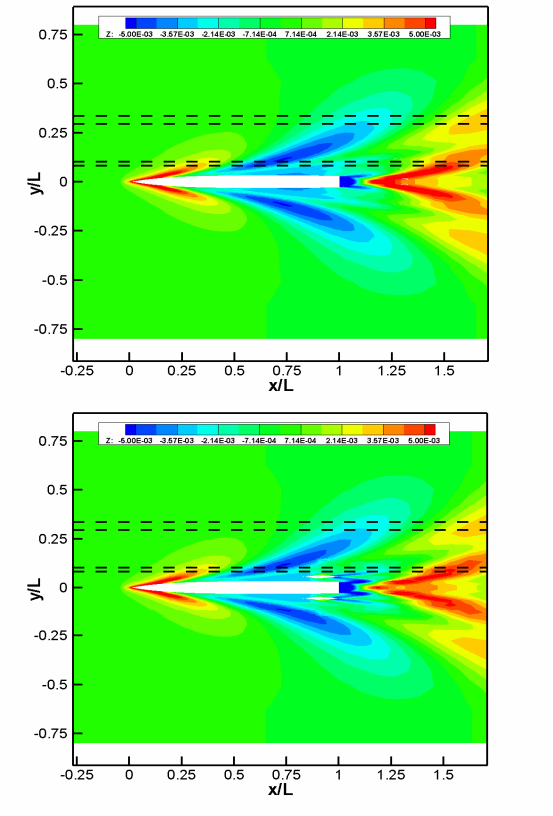

Figure 5: Computed free surface elevations: Model 5594 Trimaran (bottom) vs. Monohull (top).

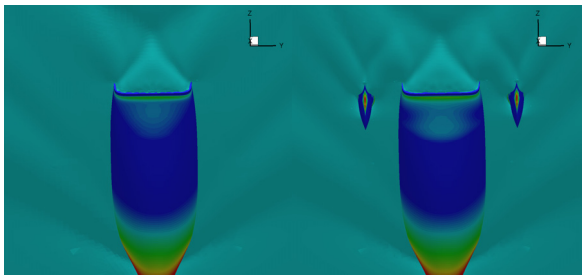

Figure 6: Hull pressure distribution: Model 5594 Trimaran (right) vs. Monohull (left).

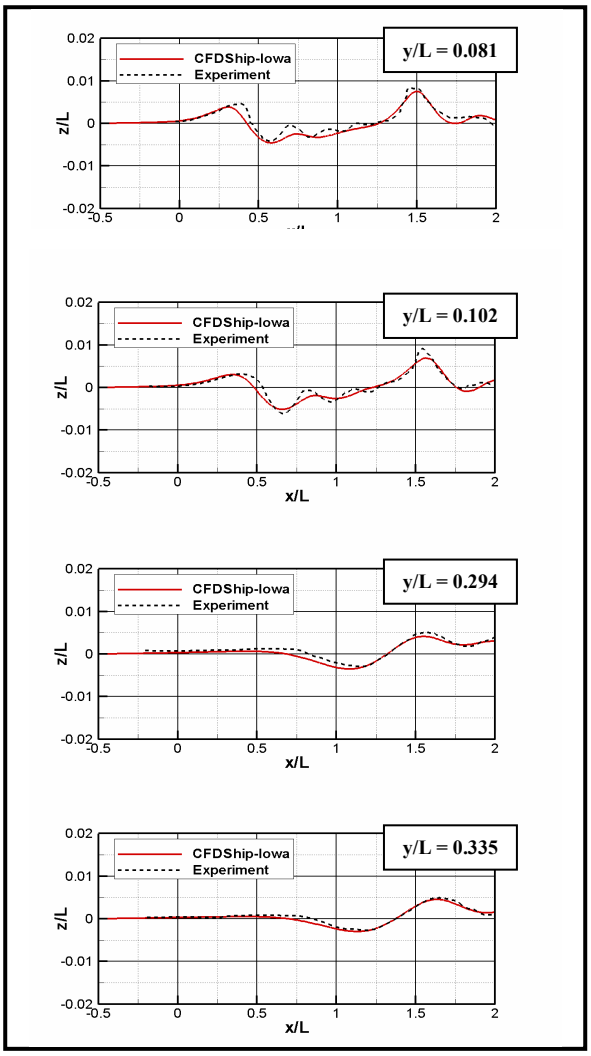

Figure 7: Model 5594 Monohull wavecuts.

Table 3 shows the individual contributions of the centerhull and sidehulls to the trimaran skin friction and the monohull (centerhull alone) skin friction at Fr = 0.511, with comparison to the ITTC values at model scale Re=3x10^7 for the centerhull and Re = 5x10^7 for the sidehulls. The small differences indicate that the RANS solver is predicting the frictional resistance very well. Table 4 shows a similar comparison for the total resistance. The static wetted areas of the monohull and trimaran are used in the respective calculated total resistance coefficients. This shows that the monohull prediction compares much better with the measured values, than the trimaran prediction. From the large differences in the errors of the monohull calculation and the trimaran calculations it appears that

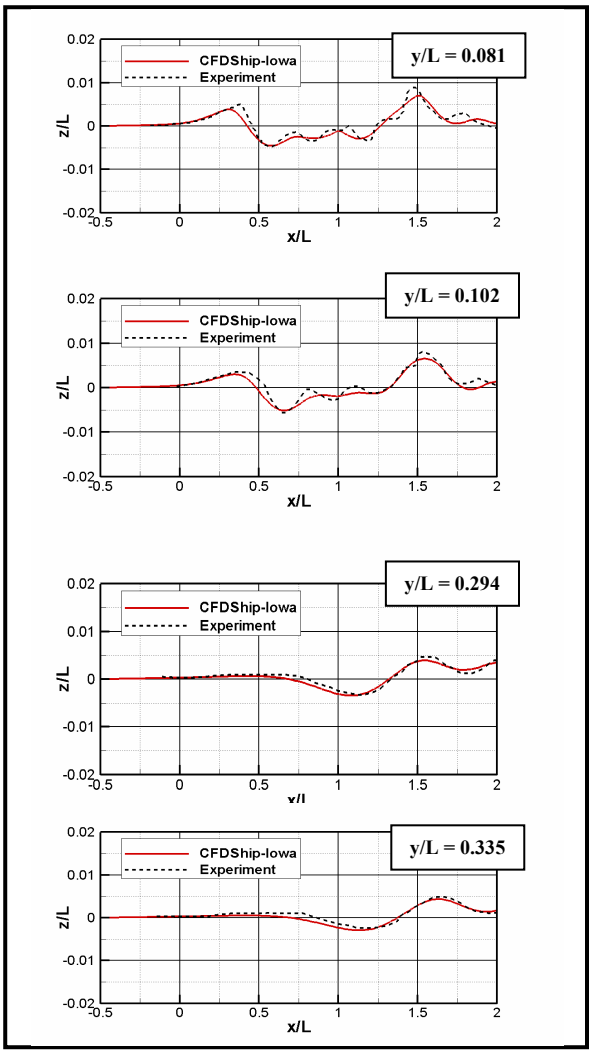

Figure 8: Model 5594 Trimaran wavecuts.

the calculation is not picking up the interference effects adequately. Figure 9 shows the comparison of the total resistance, Ct, for the entire speed range of the fixed sinkage and trim calculations. Eight speeds were calculated for the trimaran and four speeds for the monohull. The error in the total resistance of the monohull at each speed is less than 6%. A larger error is seen in the comparison with the trimaran measurements. The comparison with the trimaran is within 11% up to Fr =0.511, and then increases substantially with speed. At speeds greater than 55 kts. the calculation agrees more with the measurements from the test which included sidehull spray rails. This could occur because the RANS solver is not producing the sidehull spray that is seen in the experiment without spray rails. This spray cannot be resolved with a single-phase level set code and models would be necessary to simulate the spray effects.

Skin Friction (1000*Cf)				
		Calc	ITTC	% Difference
Trimaran	**Main hull**	2.43	2.48	1.76
	Side hull	3.46	3.37	-2.80
	Sum (Area Weighted Average)	2.54	2.55	0.55
Monohull		2.44	2.48	1.74

Table 3: Skin Friction: Trimaran vs. Monohull.

Total Resistance (1000*Ct)				
		Calc	Exp	% Difference
Trimaran	**Main hull**	3.42		
	Side hull	4.74		
	Sum (Weighted Average)	3.54	3.89	9.02
Monohull		3.48	3.64	4.32

Table 4: Total Resistance: Trimaran vs. Monohull.

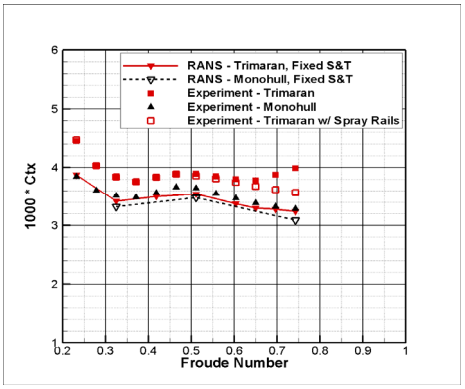

Figure 9: Predicted resistance: fixed sinkage and trim.

Predicted Sinkage & Trim, Predicted Resistance

The grid topology used for the predicted sinkage and trim calculation is the same as for the fixed sinkage and trim calculations described earlier. For these calculations, the centerhull and the sidehull grids are allowed to move (together) in response to the hydrodynamic forces. At each time step the forces and moments are calculated on the bodies, and then

integrated to obtain an adjustment to the sinkage and trim. The sinkage and trim numbers are then given to SUGGAR to update the geometry and recalculate the donor information to reassemble the grid system. Figure 10 shows the time history for the predicted sinkage, trim, and resistance for Fr = 0.55 and Fr = 0.372). This solution is started abruptly, and run until a steady state solution occurs. As seen in the figure, both the sinkage and trim are predicted very well, but the resistance is unpredicted. To compute the entire speed range the calculation was accelerated very slowly from Fr = 0.0 to Fr = 1.0 in 10,000 time steps, corresponding to a time ramp of 50 nondimensional time units. Figure 11 shows the predicted free surface elevations at 4 Froude numbers. A comparison of the predicted resistance is shown in Figure 12. As seen in figures oscillations occur at Fr < 0.40, most likely caused by a ramp not slow enough. Recall from Eq. (7) that the error is maximum at low Froude numbers.

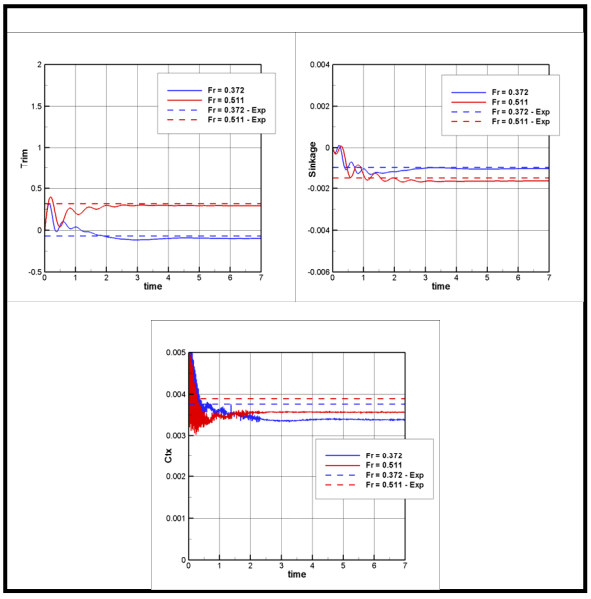

Figure 10: Predicted resistance, sinkage, & trim: Fr = 0.372 and Fr = 0.511.

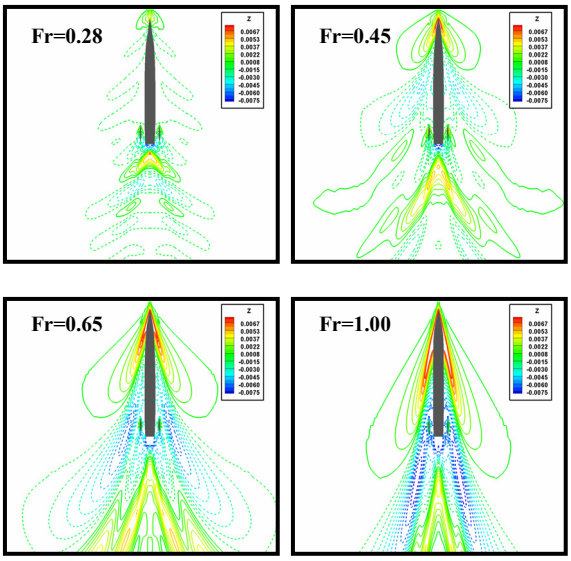

Figure 11: Calculated free surface elevations: Fr = 0.28, 0.45, 0.65, and 1.0

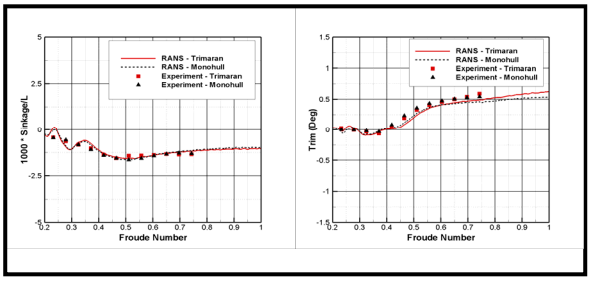

Figure 12: Predicted sinkage and trim. Solid red line: RANS trimaran, dashed black line: RANS monohull, red squares: Experiment Trimaran, black triangles: Experiment Monohull.

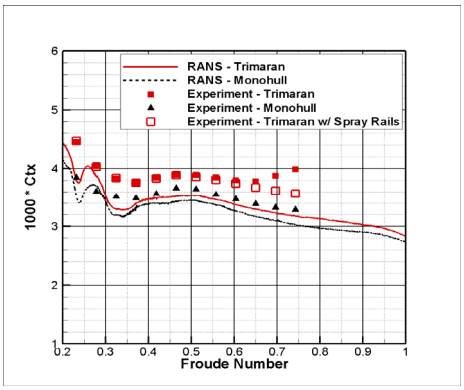

Figure 13: Predicted Resistance. Free to sink and trim.

Athena – Model 5365

The Athena R/V bare hull with skeg model 5365 was simulated in the free to sink and trim mode for a whole Froude number range from 0 to 1 using the numerical towing tank approach. Simulation results will be compared with EFD data by Jenkins (1984) including the total resistance coefficient, sinkage and trim for 10 Froude numbers ranging from 0.28 to 1.0.

In order to investigate the effect of the ramp time on CFD, two different time ramps are applied, using 50 and 100 non-dimensional seconds, respectively. It should be noted that since the velocity increases linearly as a function of time, the ship travels a total of 25 and 50 ship length, respectively. Two additional steady state points at Fr=0.5 and Fr=0.8 were also computed and put on top of the curve. A larger time step was used for the long ramp. The authors also conducted 6 steady state computations in the fixed sinkage and trim mode.

Figure 14 shows the total resistance, sinkage and trim as a function of Froude number. Analysis of equation 7 shows that the error on the Froude number evaluation is larger at lower speeds. Notice that, since we are accelerating slowly, the solution at any speed starts from a solution that is very close, and thus the one ship length necessary to develop the boundary layer and wave field to develop using Eq. (7) may be largely overestimated. This appears to be confirmed by Figure 14, which shows predictions and experimental data of resistance, sinkage and trim for Athena R/V. We can see that for an acceleration time ramp $100\,s*$ the solution is almost the same as that obtained through steady-state computations, and very close to experimental data. Beyond Fr=0.55, there is no noticeable difference of resistance coefficient between the two ramps. Steady-state solutions (Fr=0.5 and 0.8) agree very well with EFD data. As shown in Figure 14, the sinkage matches the experimental data very well for both ramps with the long ramp a little closer. For Fr<0.35, the long ramp agrees very well with the EFD data. For Fr>0.35, all trim values are under-predicted about 10%, which is likely due to an unknown error on the location of the elevation of the center of gravity (since no experimental information was available, the authors used a best guess for z_{CG}).

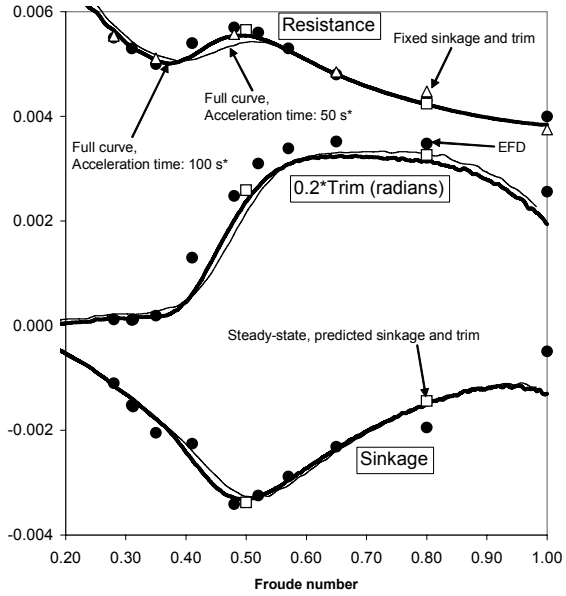

Figure 14: Results of resistance, sinkage and trim for a slow acceleration of Athena R/V barehull with skeg. Solid circles: experimental data; open triangles: resistance predictions for fixed experimental sinkage and trim; open squares: steady-state computation of resistance, sinkage and trim; fine line: acceleration in 50 s*; thick line: acceleration in 100 s*.

Free surface wave fields for four different Froude numbers (0.34, 0.43, 0.62, 1.0) are shown in Figure 15. For Fr=0.34, a classic Kelvin wave pattern is observed. With the increase of Froude number, the momentum increase results in larger spatial scale of the bow wave and larger Kelvin wave length. Compared with the RANS computation for Athena bare hull at Fr=0.43 and 0.62 (Wilson et al., 2006), the overall flow pattern is similar except for the bow wave where this study does not capture the breaking waves. Since the gird is coarse, significant diffusion of wave pattern can be observed at low Fr numbers.

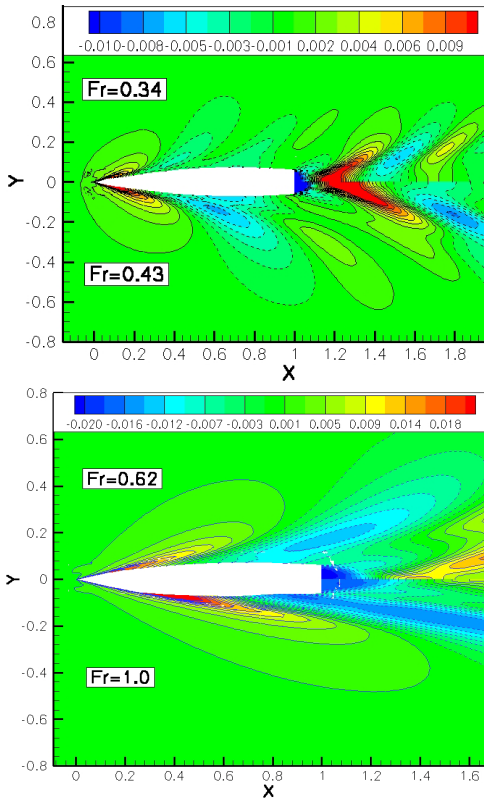

Figure 15: Free Surface wave fields Fr = 0.34, 0.43, 0.62, 1.0

Figure 16 shows wave profile heights along the ship hull for Athena R/V at four different Froude numbers. The difference between Jenkin's data and Gadd's data is Gadd's model is shorter and does not have a stern wedge. Although the authors' geometry has one, it may not be resolved due to the relative coarse grid used in this study. This probably explains why CFD agrees well with Gadd's data.

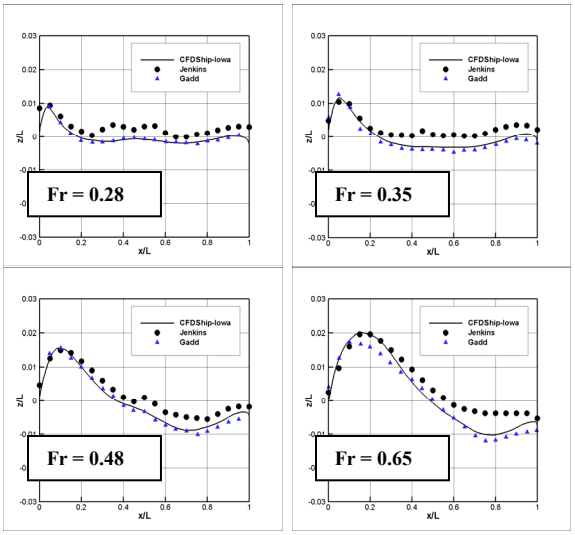

Figure 16: Comparison of predicted and measured hull wave profiles - Fr = 0.28, 0.35, 0.48, 0.65. Solid line: Calculation, Solid Dots: Jenkin's data, Triangles: Gadd's data

Athena – Appended with stabilizers, skeg, shafts, struts, and rudders

Self-propulsion of fully appended twin-screw Athena (bare hull model 4950-1 with rudder, stabilizer, skeg, shaft, shaft struts, and propeller, see Figure 17) were conducted. The software USURP was used to properly compute area and forces on overlap regions. For the different appendages, various grid topologies were used. A total of 24 blocks were used. The size of different grids for the different appendages and the grid decomposition are presented in Table 5. EFD data available, (Crook, 1981) include sinkage and trim at different Froude numbers, open water curves for thrust and torque coefficients for propeller model 4710, with corresponding propeller RPM, and thrust deduction and wake factors.

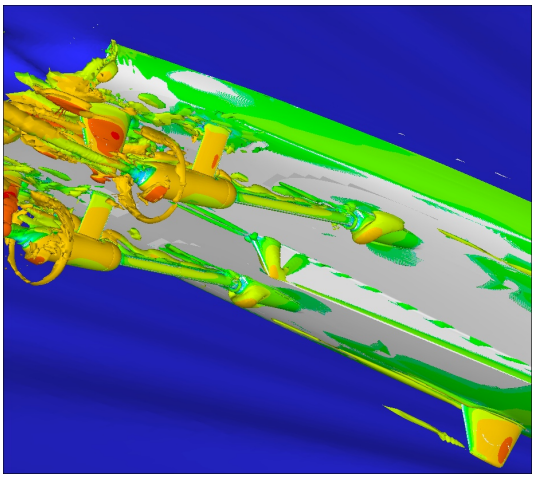

Figure 17: Athena with stabilizers, shafts, struts, and rudders (Fr=0.336, Iso-surface of Q=100, colored by streamwise velocity)

Name	# Grid Points	# Blocks	# Pts/Block
Boundary layer	351,912	3	117304
Rudder body	121,716	1	121,716
Rudder cap	39,401	1	39,401
Skeg	80,640	1	80,640
Stabilizer body	80,640	1	80,640
Stabilizer cap	38,657	1	38,657
Shaft collar	41,354	1	41,354
Shaft proper	119,600	1	119,600
Shaft cap	40,960	1	40,960
Strut left	39,701	1	39,701
Strut right	39,701	1	39,701
Wake refinement	317,520	3	317,520
Refinement	519,294	5	103858
Background	350,280	5	70056
Total Assembly	2,181,376	24	90891

Table 5: Fully Appended Athena – Grid Assembly

	Fr	Sinkage	Trim (degrees)
EFD	0.336	-0.00217	0.219
CFDSHIP	0.326 (3.0%)	-0.00169 (22%)	0.225 (2.7%)
EFD	0.576	-0.00335	1.46
CFDSHIP	0.566 (1.7%)	-0.00307 (8.4%)	1.54 (5.5%)

Table 6: Froude number, sinkage and trim predicted for a self-propelled fully appended Athena R/V.

Two steady state points were simulated (Fr=0.336, 0.576) and compared with EFD data (Table 6). The thrust, torque, and advance coefficients of the propeller are computed based on the target Fr number. The ship was initially static. When the propeller was turned on, the ship accelerated, which results in an increasing resistance force on the ship hull and appendages. When the total resistance force balanced the total thrust force from the propeller, the acceleration of the ship equals zero and the ship velocity becomes a constant. This terminal velocity (thus terminal Fr) and the predicted sinkage and trim were then compared with the target values (EFD data). From table 6, the terminal Fr numbers are within 3% error, which verify the correctness of the full scale-model scale conversion and the implementation the propeller model. Trim error is less than 6% for the two Fr numbers, while sinkage predicted is quite different from EFD data, up to 22%. The large difference for sinkage probably is due to the unknown vertical location of the center of gravity.

To view the details of the volume flow field, iso-surface of Q criterion (Hunt, 1988) is shown in Figure 17 for Fr=0.336. A tip vortex is formed in the wake of the stabilizer with a horseshoe vortex near the junction of the stabilizer and the ship hull. A steady separation bubble is formed at the trailing edge of the skeg. Shaft, struts, and rudder also create unsteady vortex shedding due to the separation. The stern is dry and the wake of the rudder causes a significant deflection of the free surface before the rooster tail. The propeller disk forms ring-like vortex tubes. To view the fluid structure at the same location, Figure 18 shows the streamlines colored by streamwise velocity. The thrust force of the propeller accelerates the flow in streamwise direction significantly. The torque force of the propeller and the tip vortex on the shaft cause the streamlines to be spiral-like in the wake of the shaft. Slices of boundary layer at different streamwise locations show that the boundary layer thickness is growing with increasing downstream, with significant effect of the appendages.

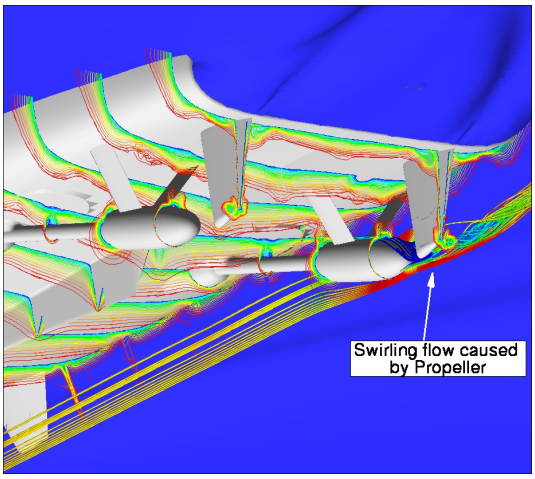

Figure 18: Boundary layer with volume streamlines in the wake near propeller

Athena fitted with a Waterjet Propulsor

Tests were performed by Chesnakas (2003) at the David Taylor Model Basin on the Athena R/V Model 5600, installed with waterjet propulsors, to investigate waterjet/hull interactions. The Model 5600 is 216 inches long, with a model scale ratio of 8.556. The waterjets were designed by a joint team of NSWCCD and Band, Lavis, and Associates. The hull and waterjet is shown in the Figure 19. The intakes for the pumps were elliptical openings at the bottom and the exits were circular on the stern of the boat. The horizontal centerline is resting on the static waterline. The axis of the pump is parallel to the ship axis. The model was tested at 8.333 kts, 16.668, and 25 kts. full speed which correspond to Fr = 0.2, 0.4, and 0.6. The model was free to sink and trim.

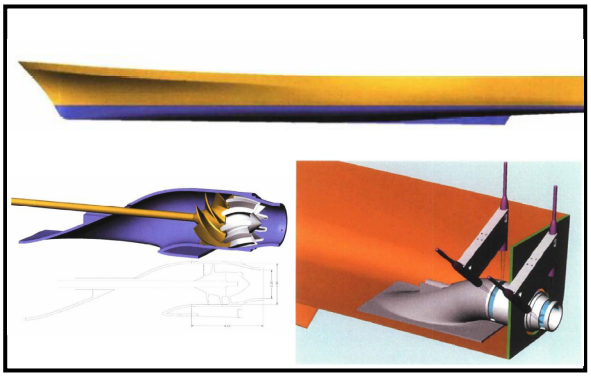

Figure 19: Sketch of the Athena R/V Model 5600 with waterjet.

Calculations simulating this experiment have started and preliminary results are presented here. Initial grids have been created to demonstrate that CFDShip-Iowa is capable of waterjet simulations. Previous waterjet calculations for this experiment include work by Ebert, et al. (2003), which did not include the above water discharge. The grid system is shown in Figure 20. The base grids consist of overlapping forward and aft hull grids and a background grid. The hull grid was split into 2 parts to facilitate the creation of the waterjet openings on the hull surface. The forward and aft volume grids are created by extruding grid lines normal to hull surfaces. Table 7 shows the grid dimensions and block splitting. The inlet and exit holes and nearby grid points in the aft grid are manually turned off in the SUGGAR run. The water jet wall surface, Figure 21, is composed of four overlapping surfaces, which also overlap the hull surface at the inlet and exit openings. The waterjet volume is discretized by extruding inward toward the center from the wall surfaces (Kandasamy, 2006). The surface assembly part of the SUGGAR process creates a water-tight hull surface from the overlapping hull and waterjet wall surfaces. Additional cartesian blocks were created near the inlet and exit to improve the quality of the resulting grid assembling. Grids to add the shaft, rotor hub, and stators are presently being created.

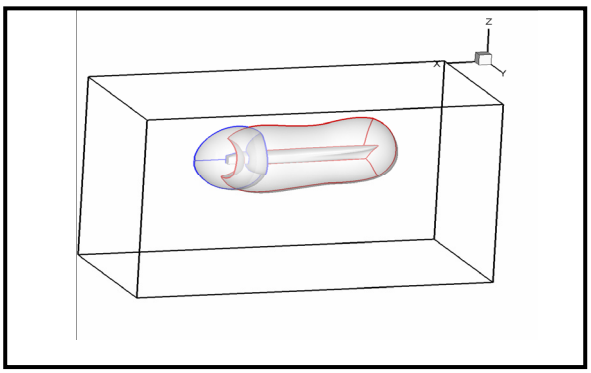

Figure 20: Athena R/V with grid extents.

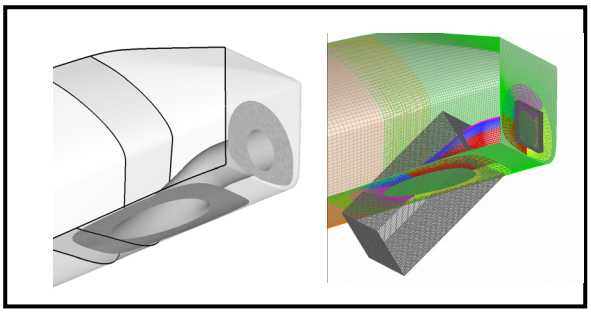

Figure 21: Athena R/V hull and waterjet surfaces.

Name	# Grid Pts	# Blocks	# Pts/Block
Waterjet Part(4)	4*109,102	4*2	109,102
Fwd Hull	1,644,000	16	102,750
Aft Hull	1,488,105	15	99,207
Inlet - Refinement	531,441	6	88,573
Exit - Refinement	155,250	2	77,625
Background	1,189,760	12	99,627
Total Assembly	5,880,656	59	Ave 99,672

Table 7: Athena R/V waterjet grid assembly.

The run conditions for this simulation correspond to the Fr = 0.6 case tested. The Reynold's Number was set to the model scale value of 2.4 x 10^7. The hull-waterjet assembly was sunk and trimmed the amount measured in the experiment. The overset grid assembler SUGGAR was run to create the final assembled grid. Since overlapping wall surfaces were used in this grid, the code USURP was run in order to calculate integrated surface quantities correctly. To demonstrate the operational waterjet, the actuator disk propulsor model thrust coefficient was varied to produce a maximum axial velocity, U/U_{inf}, of about 1.45. Axial velocity contours at different longitudinal locations are shown in Figure 22. The section showing the red ring of high velocity is located immediately aft of the actuator disk. This ring illustrates the radial extents of the applied body force. Colors inside the ring show velocites about U_{axial} = 0.9, indicating mass flow where the hub should be blocking the flow. Therefore the total mass flow through this section and any section across the jet is too high. Work is continuing to add the shaft and rotor hub to the calculation.

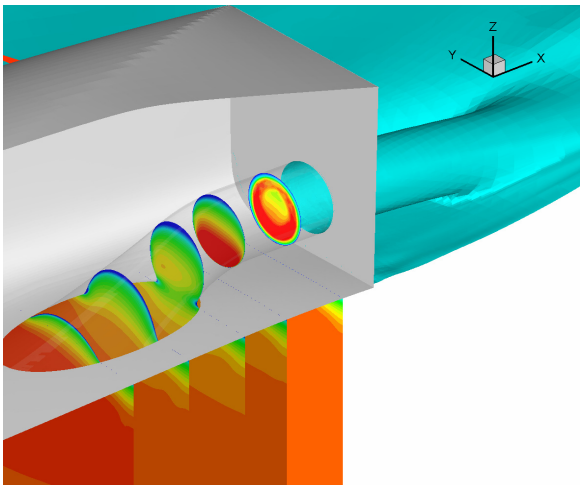

Figure 22: Athena R/V calculated axial velocity in the waterjet. The predicted is free surface is shaded cyan.

The flow entering and exiting the waterjet is shown in Figure 23. The free surface, boundary layer contours and streamlines are colored with axial velocity. Two circular jets are issued at the transom face of the ship, with significant effect on the free surface and momentum wake. To be noticed is the thinning of the boundary layer downstream of the water jet intake. A comparison of the predicted free surface wave heights for the Athena with and without waterjets in shown in Figure 22. The barehull no-waterjet configuration was calculated using the same sinkage and trim values as the jet case for comparison purposes, although more sinkage and trim will occur with an operational waterjet.

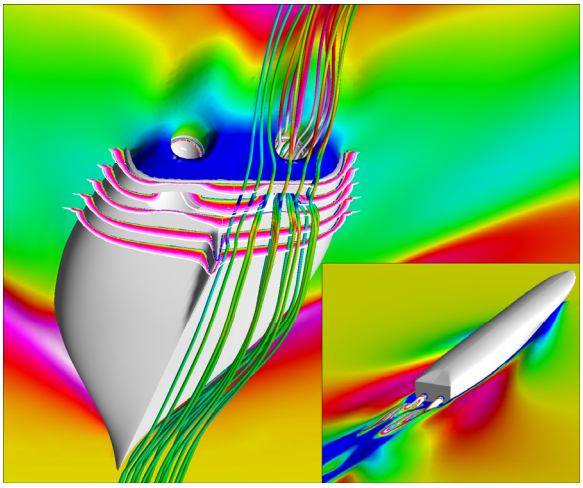

Figure 23 Athena R/V model with waterjet: Calculated free surface, boundary layer, and streamlines colored by axial velocity.

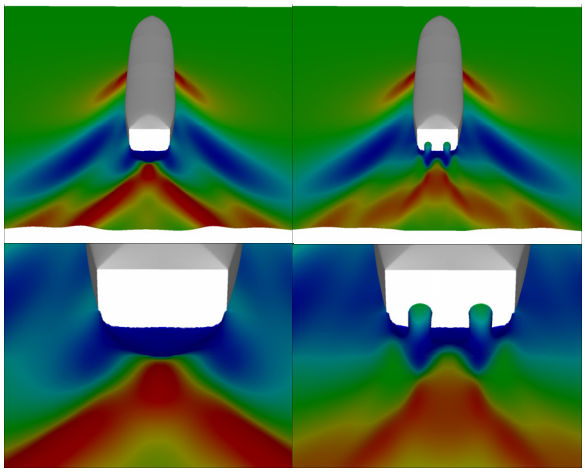

Figure 24: Athena R/V calculated free surface elevations: bare hull (left) and hull fitted with waterjets (right)

SUMMARY

RANS resistance predictions have been performed for the Athena R/V and the high speed ship Model 5594 over large ranges of speeds. For these ranges of speeds, the sinkage and trim of the hull changes substantially. Steady state cases for specific speeds throughout the range were calculated for the hulls both (1) in a fixed orientation, using the experimentally measured sinkage and trim values, and (2) free to sink and trim amounts predicted by the RANS solver. The concept of a "numerical tow tank" was used to predict the resistance, sinkage, and trim for the entire speed range by slowly accelerating the ship from Fr = 0.0 to 1.0. Resistance, sinkage, and trim curves were predicted using two different acceleration rates for the Athena R/V. Both results compared very well with the experiment, with improvement using the lower rate. Only one rate was used for the Model 5594 trimaran calculation. From the oscillations seen at low speeds, the acceleration rate was probably too high. At higher speeds, the tow tank method produced results consistent with the steady state calculations.

Self-propulsion of the Athena R/V appended with skeg, stabilizers, shafts, struts, and rudders was simulated for two Froude numbers in the free to sink and trim mode. The predicted terminal Froude number and trim agreed well with experimental data, while the amplitude of sinkage was under-predicted due to the unknown exact location of the center of gravity. It was found that the propeller significantly accelerates the fluid in the streamwise direction and generates a spiral-like vortex in the wake of the shaft.

Calculations for the Athena R/V fitted with waterjets have started, demonstrating CFDShip-Iowa's ability to simulate this configuration. The actuator disk model was turned on accelerating the flow through the jet. Streamlines and free surface plots showed the flow entering the waterjet and the above waterline discharge at the transom exit. Impact of the jet on the transom wake was illustrated. Work is continuing on this simulation by adding details of the waterjet to the grid.

ACKNOWLEDGEMENTS

The authors are grateful to the U.S. Department of Defense's High Performance Computing Modernization Program (HPCMP) office that provided the computer resources at NAVO on the IBM P4 and at ASC on the SGI O3K. The research is supported by the Office of Naval Research under the administration of Dr. Patrick L. Purtell. The NSWCCD effort is also partially supported by In-House Laboratory Independent Research (ILIR) funds under the administration of Dr. John Barkyoumb. We would like to thank Professor Yasuyuki Toda from Osaka University for his input and help in setting up the self propulsion simulation.

REFERENCES

Boger D.A. and Dreyer J.J., "Prediction of Hydrodynamic Forces and Moments for Underwater Vehicles Using Overset Grids," AIAA paper 2006-1148, 44th AIAA Aerospace Sciences Meeting, Reno, Nevada, 2006

Carrica, P.M., Wilson, R.V., Noack, R., Xing, T., Kandasamy, M., Shao, J., Stern, F., "A Dynamic Overset, Single-Phase Level Set Approach for Viscous Ship Flows and Large Amplitude Motions and Maneuvering," 26th Symposium on Naval Hydrodynamics, Rome, Italy, 17-22, September 2006a.

Carrica, P.M., Wilson, R., Stern, F., "An Unsteady Single-Phase Level Set Method for Viscous Free Surface Flows," Int. J. Num. Meth. Fluids, 2006b (in press)

Carrica, P.M., Wilson, R.V., Stern, F., "Ship Motions using Single-Phase Level Set with Dynamic Overset Grids," submitted to Comput. Fluids, 2006c.

Chesnakas, C.J., "Velocity Measurements Inside the Pump of the Gulf Coast Waterjet Tow Tank Model

5600," NSWCCD-50-TR-2003/014, February 2003, Naval Surface Warfare Center, Carderock Division.

Crook, L.B., "Powering Predictions for the R/V Athena (PG 94) Represented by Model 4950-1 with Design Propellers 4710 and 4711", David W. Taylor Naval Ship Research and Development Center, DTNSRDC/SPD-0833-05, January 1981.

Ebert, M.P, Gorski, J.J, Coleman, R.W., "Viscous Flow Calculations of Waterjet Propelled Ships," 8th International Conference on Numerical Ship Hydrodynamics, Busan, Korea, 22-25 September 2003.

Gadd, G.E., and Russell, M.J., "Measurements of the Components of resistance of a model of R.V. ATHENA," NMI R119, National Maritime Institute (Oct 1981).

Hunt, J.C.R., Wray, A.A., and Moin, P., "Eddies, Stream, and Convergence Zones in Turbulent Flows," Report CTR-S88, center for turbulent research.

Jenkins, D.S., "Resistance Characteristics of the High Speed Transom Stern Ship R/V Athena in the Bare Hull Condition, represented by DTNSRDC Model 5365", David W. Taylor Naval Ship Research and Development Center, DTNSRDC-84/024, June 1984.

Kandasamy, M., 2006, Private Communication.

Kennel, C., "Model Test Results for a 55 Knot High Speed Sealift Trimaran," Presented at RINA Design & Operation of Trimaran Ships Conference, London, 28-29 April 2004.

Menter, F.R., "Two-Equation Eddy Viscosity Turbulence Models for Engineering Applications," AIAA J., Vol. 32, 1994, pp.1598-1605.

Miller, R. W., Gorski, J.J., Wilson, R.V., Carrica, P., "RANS Simulation of a Naval Combatant Using a Single-Phase Level Set Method with Overset Grids," CFD Workshop 2005, Tokyo, Japan.

Noack R., "SUGGAR: a General Capability for Moving Body Overset Grid Assembly," AIAA paper 2005-5117, 17th AIAA Computational Fluid Dynamics Conf., Toronto, Ontario, Canada, 2005

Paterson E.G., Wilson R.V. and Stern F., "General-Purpose Parallel Unsteady RANS Ship Hydrodynamics Code: CFDShip-Iowa," IIHR report 432, Iowa Institute of Hydraulic Research, The University of Iowa, 2003

Stern, F., Kim, H.T., Patel, V.C., and Chen, H.C., "A Viscous-Flow Approach to the Computation of Propeller-Hull Interaction," Journal of Ship Research, Vol. 32, No. 4, Dec. 1988, pp. 246-262.

Wilson R.V., Carrica P.M., Stern F., "RANS Simulation of a Container Ship Using Single-Phase Level Set Method with Overset Grids," CFD Workshop 2005, Tokyo, Japan.

Wilson R.V., Carrica P.M. and Stern F., "URANS Simulations for a High-Speed Transom-Stern Ship with Breaking Waves," Int. J. CFD 2006 (in press).

Wilson, W., Fu, T.C., Pence, A.M., "Comparison of Prediction and Measured Wavefields for Model 5365 Hull Form." Naval Surface Warfare Center, Carderock Division, Hydromechanics Directorate R&D Report, NSWCCD-50-TR-2006/014, April 2006.